Exploiting Partial FDD Reciprocity for Beam Based Pilot Precoding and CSI Feedback in Deep Learning

Yu-Chien Lin, Ta-Sung Lee, and Zhi Ding

Abstract—Massive MIMO systems can achieve high spectrum and energy efficiency in downlink (DL) based on accurate estimate of channel state information (CSI). Existing works have developed learning-based DL CSI estimation that lowers uplink feedback overhead. One often overlooked problem is the limited number of DL pilots available for CSI estimation. One proposed solution leverages temporal CSI coherence by utilizing past CSI estimates and only sending CSI-reference symbols (CSI-RS) for partial arrays to preserve CSI recovery performance. Exploiting CSI correlations, FDD channel reciprocity is helpful to base stations with direct access to uplink CSI. In this work, we propose a new learning-based feedback architecture and a reconfigurable CSI-RS placement scheme to reduce DL CSI training overhead and to improve encoding efficiency of CSI feedback. Our results demonstrate superior performance in both indoor and outdoor scenarios by the proposed framework for CSI recovery at substantial reduction of computation power and storage requirements at UEs.

Index Terms—CSI feedback, FDD reciprocity, pilot placement, massive MIMO, deep learning

I. INTRODUCTION

Multiple-input multiple-output (MIMO) technology and massive MIMO are vital to 5G and future generations of wireless systems for improvement of spectrum and energy efficiency. The power of massive MIMO hinges on accurate downlink (DL) channel state information (CSI) at the basestation gNodeB (gNB). Without the benefit of uplink/downlink channel reciprocity in time-division duplxing (TDD) systems, gNB of frequency-division duplexing (FDD) systems typically relies on user equipment (UE) feedback to acquire DL CSI. The extraordinarily large number of DL transmit antennas envisioned in millimeter wave or terahertz bands in future networks [1] places a tremendous amount of feedback burden on uplink (UL) resources such as bandwidth and power. As a result, CSI feedback reduction is crucial to widespread deployment of massive MIMO technologies in FDD systems.

Y.-C Lin is with the Department of Electrical and Computer Engineering, University of California at Davis, Davis, CA, USA, and was affiliated with National Yang Ming Chiao Tung University, Taiwan (e-mail: ycm-lin@ucdavis.edu).

Since CSI in most environments has limited delay spread and can be viewed as sparse, CSI feedback by UEs can take advantage of such low dimensionality for CSI feedback compression. To extract CSI sparsity for improved feedback efficiency, the work [2] first proposed a deep autoencoder framework by deploying encoders and a decoder at UEs and the serving base station, respectively, for CSI compression and recovery. This and other related works have demonstrated significant performance improvement of CSI recovery with the use of deep learning autoencoder [3]–[5].

In addition to autoencoder for direct DL CSI feedback and recovery, recent works leveraged correlated channel information such as past CSI [6], [7], CSI of nearby UEs [8], and UL CSI [9]-[11] to improve the recovery of DL CSI at base stations. Specifically, physical insights considering slow temporal variations of propagation scenarios, similar propagation conditions of similarly located UEs, and similarity of UL/DL radiowave paths reveal significant temporal, spatial, and spectral CSI correlations respectively. More strikingly, UL CSI is generally available at gNB in existing FDD wireless networks and is easier to utilize in practice. In addition, FDD reciprocity in magnitudes is not only shown from dats generated by CSI models [10] but was also later verified in measurement [12]. Other related works also considered antenna array geometry to exploit the UL/DL angular reciprocity to improve DL CSI estimation in FDD wireless systems [13], [14]. The work [13] exploited UL/DL angular reciprocity in designing an adaptive dictionary learning for seeking the sparse representation of DL CSIs for feedback. The reciprocity is also utilized for directional training to enhance DL CSI estimation in [14].

Instead of CSI recovery, a related approach [15]–[18] is to exploit FDD reciprocity and angular sparsity to directly determine precoding matrix for reducing feedback overhead. The authors [15] propose an AoD-adaptive subspace codebook framework for efficiently quantizing and feeding back DL CSI. The 5G (NR) supports Type I [16] and Type II [17] codebooks corresponding to low- and high-resolution beams, respectively. The optimum serving beam can be selected by feeding back a predetermined codebook with the largest response between the UE and gNB. Similarly, instead of feeding back predetermined codebook, another idea in [18] is for UE to feed back compressed singular vectors corresponding to the dominant singular values for precoding matrix optimization.

Importantly, the estimation accuracy of DL CSI at UEs depends on several factors such as channel fading properties and reference signal (RS) placement. Beyond feedback overhead, the required resource pilot (i.e. CSI-RS) allocation

Z. Ding is with the Department of Electrical and Computer Engineering, University of California, Davis, CA, USA (e-mail: zding@ucdavis.edu).

T.-S Lee is with the Institute of Communications Engineering, National Yang Ming Chiao Tung University, Taiwan (e-mail: tslee@mail.nctu.edu.tw).

This work is based on materials supported by the National Science Foundation under Grants 2029027 and 2002937 (Lin) and by the Center for Open Intelligent Connectivity under the Featured Areas Research Center Program within the framework of the Higher Education Sprout Project by the Ministry of Education (MOE) of Taiwan, and partially supported by the Ministry of Science and Technology (MOST) of Taiwan under grant MOST 110-2634-F-009-028 and MOST 110-2224-E-A49-001 (Lee and Lin).

for CSI estimation also grows proportionally with the antenna array size. More resource allocated to CSI-RS would improve DL CSI estimation accuracy but degrade spectrum efficiency. In practical systemsW such as [19], CSI-RS resources are sparsely allocated on time-frequency physical resource grid. To our best knowledge, only a few studies [20], [21] considered the sparse CSI-RS availability in designing CSI feedback mechanisms. The deep learning partial CSI feedback framework proposed by [20] reduces RS resource overhead by leveraging temporal CSI correlation. In the work of [21], the gNB optimizes the DL pilot values (i.e., CSI-RS) based on UL CSI without reducing the CSI-RS resources. However, such implementation would require dynamic exchange of optimized pilot values between the gNB and the UE and is incompatible with the present use of predefined CSI-RS.

In this work, we aim to reduce DL CSI-RS overhead and the UL feedback overhead while maintaining DL CSI recovery accuracy at gNB by exploiting the available UL CSI. We develop an efficient and reconfigurable deep learning beam based CSI feedback framework by leveraging UL/DL angular reciprocity for FDD wireless systems. Our contributions are summarized as follows:

- The framework proposes a beam-space precoding approach to exploit the FDD UL/DL reciprocity in beam response magnitudes and generate a low-dimensional representation that is easier to recover with fewer antenna ports (APs), leading to lower DL CSI training and UL feedback overhead.
- The framework reconfigures CSI-RS placement by reducing either pilot resource density or the number of APs without loss of CSI recovery accuracy. An UL feedback overhead compression module further reduces UL feedback overhead.
- The framework better utilizes FDD reciprocity by not only feeding UL CSI magnitudes as deep learning inputs [10], but also designing a beam-based precoding matrix according to high similarity of UL/DL beam response magnitudes.
- The reduction of DL CSI training overhead in the framework can significantly lower the computation and storage burdens related to the compression by the low cost UEs given the input size reduction of the compression module.

We let $(\cdot)^H$, $(\cdot)^T$ denote conjugate transpose and transpose operations, respectively. $(\cdot)^*$ denotes complex conjugate. The i-th column of $N \times N$ identity matrix \mathbf{I} is the unit vector \mathbf{e}_i .

II. SYSTEM MODEL

We consider a single-cell MIMO FDD link in which a gNB using a $N_H \times N_V$ uniform planar array (UPA) with $N_b = N_V N_H$ antennas communicates with single antenna UEs. Focusing on a specific UE, the DL subband consists of K resource blocks (RBs) for DL CSI-RS and data transmission. We assume channels within an RB to be under slow, flat and block fading. As shown in Fig. 1, there are $N_f \times N_O$ time-frequency resource elements (REs) in a specific RB

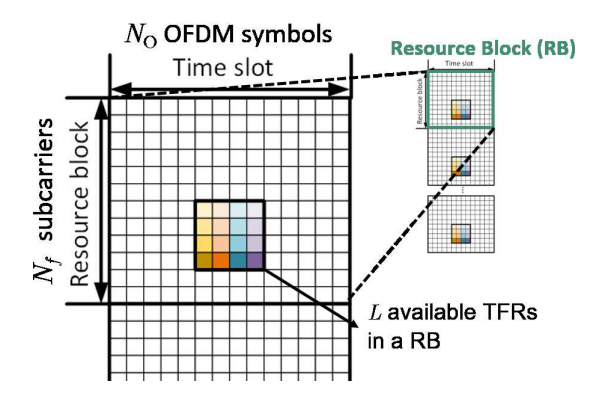


Fig. 1. Resource block configuration.

 $(N_{\rm f} \ {
m subcarriers} \ {
m and} \ N_{
m O} \ {
m OFDM} \ {
m symbols}).$ Since the same processing procedures are applied for every RB, without loss of generality, we only discuss the processing in a single RB in this section. Given that the gNB assigns N_b REs for DL CSI training for N_b antennas, the received signal vector ${
m y}_{
m DL} \in \mathbb{C}^{N_b \times 1}$ at UE can be expressed as

$$\mathbf{y}_{\mathrm{DL}} = \mathbf{S}_{\mathrm{DL}, N_b} \cdot \mathbf{h}_{\mathrm{DL}} + \mathbf{n}_{\mathrm{DL}},\tag{1}$$

where $\mathbf{h}_{\mathrm{DL}} = \mathrm{vec}(\mathbf{H}_{\mathrm{DL}}) \in \mathbb{C}^{N_b \times 1}$ denotes the DL CSI vector whereas $\mathbf{S}_{\mathrm{DL},N_b} = \mathrm{diag}(\mathbf{s}_{\mathrm{DL}}) \in \mathbb{C}^{N_b \times N_b}$ denotes the CSI-RS training symbol matrix which is diagonal matrix with diagonal entries of training symbols $s_{\mathrm{DL}}^{(n)}, n = 1, ..., N_b.$ $\mathbf{n}_{\mathrm{DL}} \in \mathbb{C}^{N_b \times 1}$ denotes the additive noise. $\mathbf{H}_{\mathrm{DL}} \in \mathbb{C}^{N_H \times N_V}$ denotes the DL CSI matrix before reshaping. From known training symbols in $\mathbf{S}_{\mathrm{DL},N_b}$, the UE can estimate its DL CSI for feedback to gNB via

$$\widehat{\mathbf{h}}_{\mathrm{DL}} = \mathbf{S}_{\mathrm{DL}, N_b}^{-1} \cdot \mathbf{y}_{\mathrm{DL}}.\tag{2}$$

A. Beam-Space (BS) Precoding and DL CSI recovery

Existing wireless systems [19], [22] have applied beamforming/precoding techniques to CSI-RS symbols for beam selection, DL CSI estimation, or resistance to attenuation in high frequencies. In this work, we consider DL CSI recovery at gNB under beamforming, which serves as CSI performance baseline. According to [23], we can find N_b orthogonal beams to construct an unitary "orthogonal beam matrix (OBM)" $\mathbf{B} = [\mathbf{b}^{(1)} \ \mathbf{b}^{(2)} \ ... \ \mathbf{b}^{(N_b)}]$. As shown in Fig. 2.A, applying the OBM to the CSI-RS matrix $\mathbf{S}_{\mathrm{DL},N_b}$ in the digital beamforming module, the UE receives signals at different REs:

$$\mathbf{y}_{\mathrm{DL}} = \mathbf{S}_{\mathrm{DL}, N_b} \mathbf{B}^T \mathbf{h}_{\mathrm{DL}} + \mathbf{n}_{\mathrm{DL}}. \tag{3}$$

From the orthogonality of the OBM, the DL CSI can reconstructed at the gNB from the quantized feedback $\bar{\mathbf{g}}_{\mathrm{B}} = Q(\mathbf{S}_{\mathrm{DL},N_b}^{-1}\mathbf{y}_{\mathrm{DL}})$ from the UE according to the CSI-RS information \mathbf{s}_{DL} as follows:

$$\widehat{\mathbf{h}}_{\mathrm{DL}} = \mathbf{B}^* \bar{\mathbf{g}}_{\mathrm{B}} = \mathbf{B}^* Q(\mathbf{S}_{\mathrm{DL}, N_b}^{-1} \mathbf{y}_{\mathrm{DL}}), \tag{4}$$

where $Q(\cdot)$ denotes the encoding process (e.g. quantization). Given the angular sparsity of DL CSIs, especially for DL CSIs in line-of-sight (LOS) scenarios, the beam space (BS) DL CSI $\mathbf{h}_{\mathrm{BS,DL}}(=\mathbf{B}^T\mathbf{h}_{\mathrm{DL}})$ can be assumed as a L-sparse vector

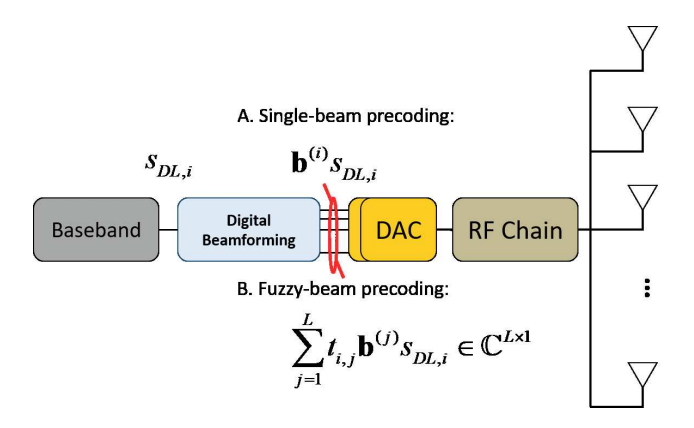


Fig. 2. Signal processing flow for beam-space precoding

and thus DL CSI \mathbf{h}_{DL} can be approximated according to the most significant L ($L < N_b$) beams as follows:

$$\widehat{\mathbf{h}}_{\mathrm{DL}} = \mathbf{B}_{\mathrm{S}}^* \bar{\mathbf{g}}_{\mathrm{B,S}} \tag{5}$$

where $\mathbf{B}_{\mathrm{S}} \in \mathbb{C}^{N_b \times L}$ and $\bar{\mathbf{g}}_{\mathrm{B,S}} \in \mathbb{C}^{L \times 1}$ respectively denote the significant beam matrix consisting of the steering vectors of the most significant L orthogonal beams, and the corresponding quantized beam responses. Our experiments show that, in propagation channels with low angular spread, the top 1/4 beams approximately contribute to 90% of DL CSI energy in beam domain. Relying on L significant beams, the gNB only need to assign L ($< N_b$) REs for CSI-RS in DL to reduce UL feedback.

Typically, the L significant beams could be found through beam training or direction finding [24]–[26] by utilizing additional bandwidth and power resources. Fortunately, the FDD UL/DL reciprocity in magnitudes of angular CSI [10] can help gNB implement this beam selection process by relying the available UL CSI at gNB. The numerical test results of Fig. 3 illustrate the recovery performance of DL CSI by determining precoding matrix \mathbf{B}_{S} which consists of the L significant beams selected according to CSI magnitudes in UL and DL beam domains, respectively. The modest difference in terms of CSI estimation error demonstrates the high correlation (reciprocity) between CSI magnitudes in UL and DL beam domains. Specifically, the L dominant beams of UL and DL channels are highly correlated. Good CSI recovery performance requires sufficient number of beams L or REs for CSI-RS.

III. BS PRECODING AND DL CSI RECOVERY

A. Single-beam Precoding and DL CSI Recovery

As seen from the preliminary results of Fig. 3, CSI recovery accuracy hinges on the number of available REs (equal to the number of selected beams). Namely, missing beam responses of the non-selected beams cause performance degradation. On the other hand, careful examination of the DL CSI in beam domain, we note the significant spatial correlation between vertically and horizontally adjacent beam responses. Equally important is the fact that UL CSI magnitudes can help improve DL CSI estimation.

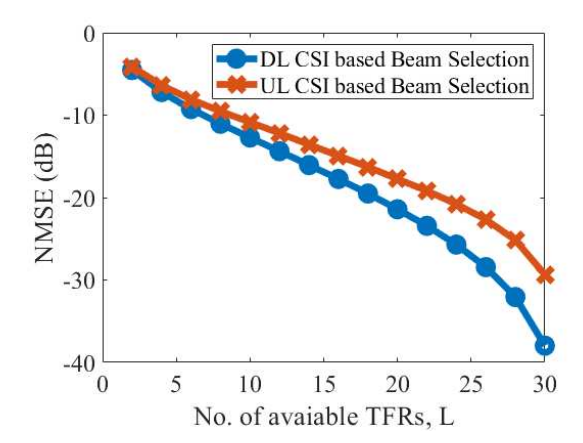


Fig. 3. Normalized mean square error (NMSE) of the recovered results obtained by beam selection according to UL/DL CSI magnitudes. (This experiment is based on simulated outdoor UMa channels generated by QuadDRiGa channel simulator [27].)

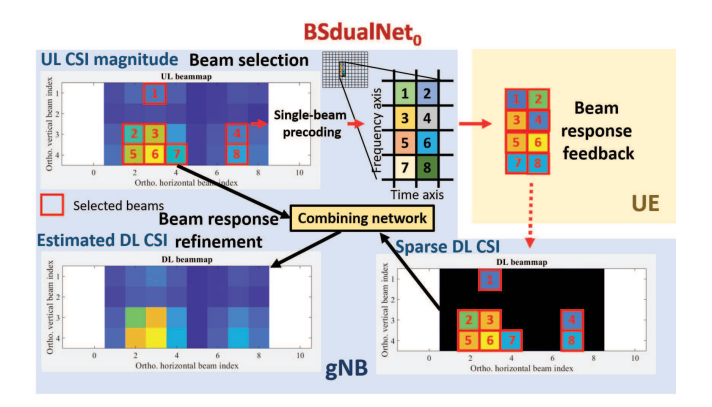


Fig. 4. Illustration of BSdualNet₀.

Taking advantage of these insights, we first develop a heuristic CSI feedback framework, *BSdualNet*₀. As shown in Fig. 4, the BSdualNet₀ consists of three phases:

- *UL-CSI aided beam selection*: the gNB selects L beams with the largest responses in UL CSI by assigning training symbols on L REs for CSI-RS transmission to UEs. We denote the index set of these beams as $\Omega_{\rm B}$.
- Beam response feedback: the UE estimates the beam responses for direct encoding and feedback to the gNB.
- Beam response refinement: the gNB first generates a sparse map filled with the quantized beam responses according to the index set of the selected beams Ω_B . The sparse map and local UL CSI magnitudes form inputs to a deep learning network to estimate the missing elements in the sparse map for DL CSI refinement. The deep neural network (DNN) generates refined DL beam domain CSI.

B. BS Precoding and DL CSI Recovery

We also develop a BS DL CSI recovery framework which assigns N_b orthogonal beams to L REs ($L < N_b$). Instead of utilizing a single beam for each RE, as shown in Fig. 2.B, a combination of weighted beams is applied. Let us denote an

 $N_b \times L$ beam merging matrix

$$\mathbf{T} = \begin{bmatrix} \mathbf{t}_1 & \mathbf{t}_2 & \dots & \mathbf{t}_L \end{bmatrix}, \quad \mathbf{t}_i = \begin{bmatrix} t_{1,i} \\ \vdots \\ t_{N_b,i} \end{bmatrix}. \tag{6}$$

The received signal vector at UE is expressed as

$$\mathbf{y}_{\text{DL}} = \begin{bmatrix} \sum_{i=1}^{N_b} t_{i,1} \mathbf{h}_{\text{DL}}^T \mathbf{b}^{(i)} s_{\text{DL}}^{(1)} \\ \sum_{i=0}^{N_b-1} t_{i,2} \mathbf{h}_{\text{DL}}^T \mathbf{b}^{(i)} s_{\text{DL}}^{(2)} \\ \vdots \\ \sum_{i=0}^{N_b-1} t_{i,L} \mathbf{h}_{\text{DL}}^T \mathbf{b}^{(i)} s_{\text{DL}}^{(L)} \end{bmatrix} + \mathbf{n}_{\text{DL}}$$

$$= \begin{bmatrix} \mathbf{h}_{\text{DL}}^T \mathbf{B} \mathbf{t}_1 s_{\text{DL}}^{(1)} \\ \mathbf{h}_{\text{DL}}^T \mathbf{B} \mathbf{t}_2 s_{\text{DL}}^{(2)} \\ \vdots \\ \mathbf{h}_{\text{DL}}^T \mathbf{B} \mathbf{t}_L s_{\text{DL}}^{(L)} \end{bmatrix} + \mathbf{n}_{\text{DL}}$$

$$= \mathbf{S}_{\text{DL},L} \mathbf{T}^T \mathbf{B}^T \mathbf{h}_{\text{DL}} + \mathbf{n}_{\text{DL}} = \mathbf{S}_{\text{DL},L} \mathbf{T}^T \mathbf{h}_{\text{BS,DL}} + \mathbf{n}_{\text{DL}},$$

where **T** is used to reduce the required REs and to find a compact representation of DL CSI. $\mathbf{h}_{\text{BS,DL}} = \mathbf{B}^T \mathbf{h}_{\text{DL}}$ denotes the DL CSI vector in beam domain. The raw and quantized response vectors of the merged beam responses are denoted by $\mathbf{g}_{\text{FB}} = \mathbf{S}_{\text{DL},L}^{-1} \mathbf{y}_{\text{DL}}$ and $\bar{\mathbf{g}}_{\text{FB}} = Q(\mathbf{g}_{\text{FB}})$, respectively.

Our goal is to find a beam merging matrix $\mathbf{T} \in \mathbb{C}^{N_b \times L}$ and a mapping function f_{re} for recovering the DL CSI based on the quantized feedback vector via the principle of

$$\arg\min_{\mathbf{T}, \mathcal{Q}_{r}} ||\mathbf{B}^* f_{re}(Q(\mathbf{S}_{DL,L}^{-1} \mathbf{y}_{DL})) - \mathbf{h}_{DL}||_F^2$$
(8)

where Ω_{re} denotes the deep learning model parameters to be optimized. Following this principle, the detailed design and architecture of an UL CSI-aided feedback framework for DL CSI estimation will follow in the next section.

IV. ENCODER-FREE CSI FEEDBACK WITH UL CSI ASSISTANCE

In this section, we start with the general architecture of the two proposed frameworks (*BSdualNet*, *BSdualNet-MN*). Both exploit UL/DL reciprocity to design the beam merging matrix **T** for dimension reduction but utilize different recovery schemes. Next we introduce detailed model learning objectives and design principle. Note that, unlike the previous learning-based frameworks, DNN encoders are not necessary to be deployed on the UEs, thereby reducing memory and computation burdn on low cost UEs. Instead, this new framework lowers the required REs for CSI-RS of DL MIMO channels and reduces UL feedback overhead.

A. General Architecture

For simplicity, Fig. 5 shows the general architecture of the proposed CSI feedback framework for a single-UE, though the same principle applies for multiple UEs. Consider a wireless communication system with L REs assigned in each RB for CSI-RS placement. We first design a beam merging matrix

T to match N_b orthogonal beams with different weights to the L REs that carry CSI-RS for dimension reduction. We use a beam merging network that use UL CSI magnitudes in beam domain as inputs. Owing to the high correlation between magnitudes of UL and DL CSIs in beam domain, the beam merging network learn to assign suitable weights to orthogonal beams according to the UL CSI magnitudes $|\mathbf{B}^T\mathbf{h}_{\text{UL}}|$ in BS that are locally available at gNB. Next, we apply the beam merging matrix T to L CSI-RS symbols the L REs. Consequently, the effective channels at UEs after CSI estimation would be the weighted sum of beam responses as estimate of the full CSI at downlink. Obtaining effective channels, the UE simply quantize and feeds back the channel information to the gNB. The gNB recovers DL CSI by sending the quantized feedback and the known beam merging matrix T into the proposed deep learning decoder network.

Unlike previous works, our new framework does not require another encoder at UE to store and compress full DL CSI. This is beneficial to UE devices with limited computation, storage, and/or power resources. Moreover, we reduce the DL overhead of CSI-RS and provide higher spectrum efficiency. In addition, the linear mapping matrix \mathbf{T} instead of a general or nonlinear mapping function $f: \mathbb{C}^{N_b} \to \mathbb{C}^L$ for pilot dimension reduction provides the advantage of simpler implementation and easier decoupling of CSI-RS symbols.

B. BSdualNet

Fig. 6 shows the proposed CSI feedback framework, BSdualNet, in multi-user scenarios (i.e., N UEs). As shown in Fig. 7, we aggregate and reshape the magnitudes of BS UL CSIs of each UE into a tensor $|\mathcal{H}_{BS,UL}| \in \mathbb{C}^{N_H \times N_V \times N}$, which is sent to the beam merging network. The beam merging deep learning network (Fig. 7) consists of four 3×3 circular convolutional layers with 16, 8, 4, and 2 channels, respectively, to learn the importance of different orthogonal beams according to the spatial structures of UL beam domain CSI magnitudes. Given the circular characteristic of BS CSI matrices, we introduce circular convolutional layers to replace traditional convolution. Subsequently, a fully connected (FC) layer with $2N_bL$ elements is included to generate desired dimension after reshaping (Recall that T is a complex matrix with size of $N_b \times L$). After CSI estimation at UEs, the gNB receives the N copies of quantized feedbacks from N UEs and obtains quantized feedbacks $\bar{\mathbf{g}}_{\mathrm{FB}}^{(i)} \in \mathbb{C}^{2L}, i=1,2,\ldots,N.$

Now we focus on the network at gNB. For the i-th UE, we forward the received feedback $\bar{\mathbf{g}}_{FB}^{(i)}$ to a FC layer with $2N_b$ elements. After reshaping the feedback data into a matrix of size $N_H \times N_V \times 2$, we use four 3×3 circular convolutional layers with 16, 8, 4, and 2 channels and activation functions to generate initial BS DL CSI estimate $f_{re}(\bar{\mathbf{g}}_{FB}^{(i)})$. Next, the gNB forwards the initial BS DL CSI estimate $f_{re}(\bar{\mathbf{g}}_{FB}^{(i)})$ to together with the BS UL CSI magnitudes $|\mathbf{H}_{BS,UL}^{(i)}|$ to the combining network for final DL CSI estimation. The combining network uses N_B residual blocks, each block contains the same design of circular convolutional layers and activation functions as the network for DL CSI recovery.

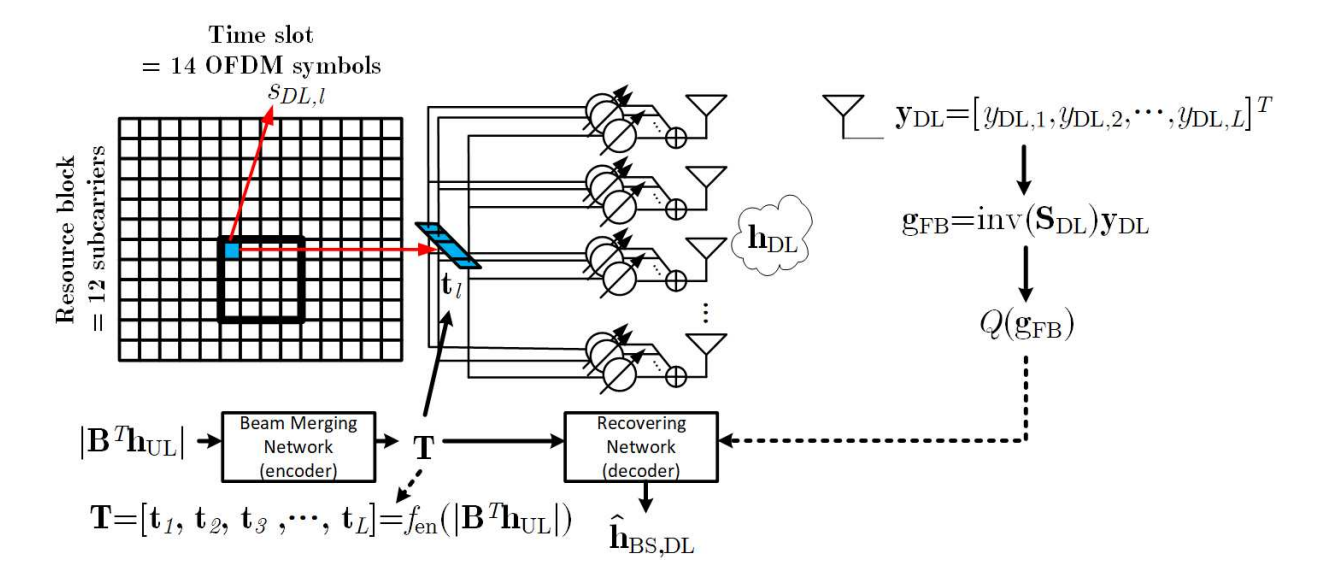


Fig. 5. General architecture of the proposed BS CSI feedback framework. (Each of the small grids is a TFR. The region covered by the bold black frame is the designated place for RS replacement. Thus, in this example, the available number of TFRs, L, is 16.)

The BSdualNet is optimized by updating the network parameters $\Theta_{\rm bm}$, $\Theta_{\rm re}$ and $\Theta_{\rm c}$ of non-linear beam merging, recovery, and combining networks $f_{\rm bm}$, $f_{\rm re}$ and $f_{\rm c}$:

$$\underset{\Theta_{\text{bm}},\Theta_{\text{re}},\Theta_{c}}{\arg\min} \left\{ \sum_{i=0}^{N-1} \left\| \widehat{\mathbf{h}}_{\text{BS,DL}}^{(i)} - \mathbf{h}_{\text{BS,DL}}^{(i)} \right\|_{F}^{2} \right\}, \tag{9}$$

$$\hat{\mathbf{h}}_{\text{BS,DL}}^{(i)} = f_{\text{c}}(f_{\text{re}}(\bar{\mathbf{g}}_{\text{FB}}^{(i)}), |\mathbf{H}_{\text{BS,UL}}^{(i)}|),$$
 (10)

$$\bar{\mathbf{g}}_{FB}^{(i)} = Q((\mathbf{S}_{DL,L}^{(i)})^{-1} \mathbf{y}_{DL}^{(i)}), \tag{11}$$

$$\mathbf{y}_{\text{DL}}^{(i)} = \mathbf{S}_{\text{DL},L}^{(i)} \mathbf{T} \mathbf{h}_{\text{BS,DL}}^{(i)} + \mathbf{n}_{\text{DL}}^{(i)},$$
 (12)

$$\mathbf{T} = f_{\text{bm}}(|\mathbf{h}_{\text{BS,UL}}^{(1)}|, |\mathbf{h}_{\text{BS,UL}}^{(2)}|, ..., |\mathbf{h}_{\text{BS,UL}}^{(N)}|). \tag{13}$$

Note that the superscript $^{(i)}$ denotes the UE index. $\mathbf{h}_{\mathrm{BS,UL}}^{(i)} = \mathrm{vec}(\mathbf{H}_{\mathrm{BS,UL}}^{(i)}) \in \mathbb{C}^{N_HN_V}$ and $\mathbf{H}_{\mathrm{BS,UL}}^{(i)} \in \mathbb{C}^{N_H \times N_V}$ denote the vectorized and original UL CSI in beam domain at the i-th UE.

C. BSdualNet-MN

In BSdualNet, the beam merging network provides a beam merging matrix **T** to generate an efficient representation of the convoluted responses of all orthogonal beams. Although **T** is optimized for the ease of decoupling individual beam responses, the decoder remains a blackbox such that the information within **T** may not be fully exploited due to its indirect use. In this section, we would redesign the decoder by directly using the beam merging matrix **T** to achieve better architectural interpretability and performance improvement.

Unlike the previous works that split the deployment of CSI encoder and decoder at UEs and gNB, respectively, our gNB knows the exact encoding and decoding processes in our framework. Thus, we can exploit the locally known beam merging matrix **T** to decode the feedback more efficiently. To

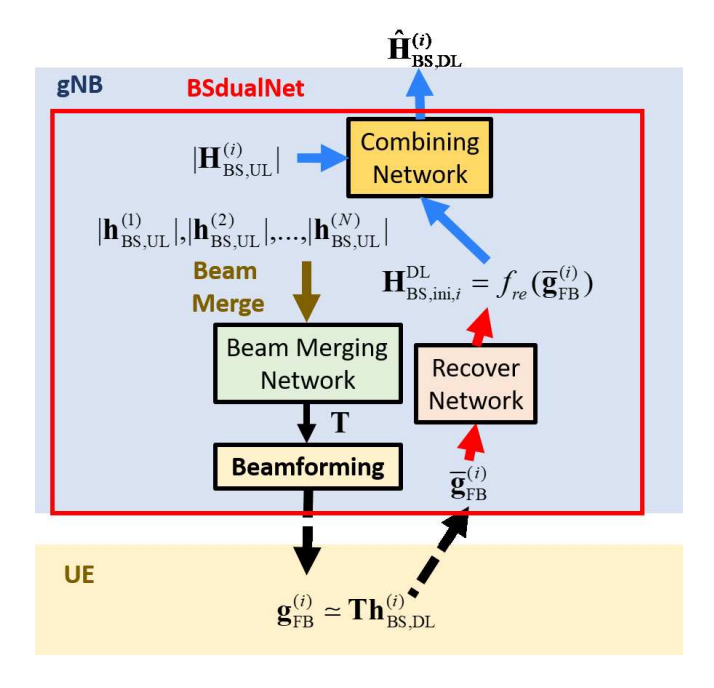


Fig. 6. Block Diagram of BSdualNet.

this end, we reformulate the problem of DL CSI recovery for $\widehat{\mathbf{h}}_{\mathrm{BS,DL}}^{(i)}, i=0,...,N-1$ by seeking a minimum-norm solution to an under-determined linear system

$$\mathbf{y}_{\mathrm{DL}}^{(i)} = \mathbf{T}^{T} \mathbf{h}_{\mathrm{BS,DL}}^{(i)} + \mathbf{n}_{\mathrm{DL}}^{(i)}, i = 0, ..., N-1.$$

As seen from Fig. 8, the output of the recovery network can be expressed as follows:

$$f_{\text{re}}(\widetilde{\mathbf{g}}_{\text{FR},i}^{(i)}) = \mathbf{T}^H (\mathbf{T}\mathbf{T}^H)^{-1} \widetilde{\mathbf{g}}_{\text{FR}}^{(i)}, \tag{14}$$

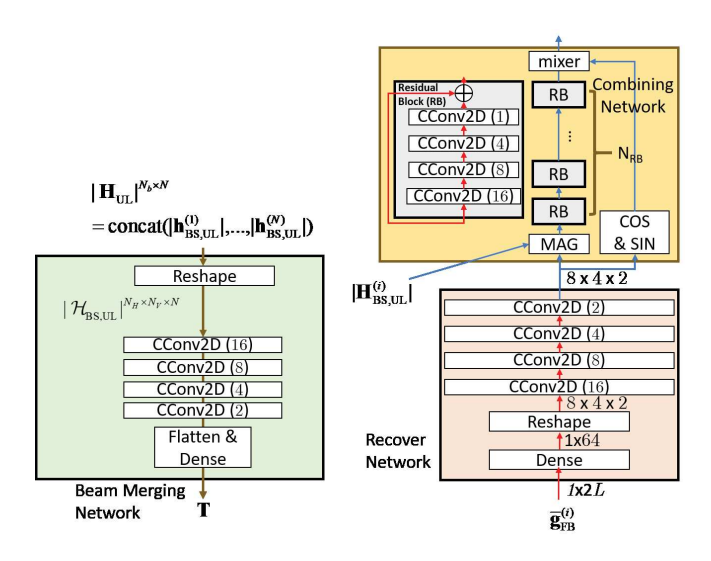


Fig. 7. Network design of BSdualNet.

Clearly, the minimum norm solution depends on matrix T. Assuming perfect quantization and zero noise, we can approximate the decoder¹ of Eq. (14) as

$$f_{\text{re}}(\widetilde{\mathbf{g}}_{\text{FB}}^{(i)}) \approx \mathbf{T}^{H}(\mathbf{T}\mathbf{T}^{H})^{-1}\mathbf{T}\mathbf{h}_{\text{BS,DL}}^{(i)},$$

$$= \underbrace{\sum_{i=1}^{L} \mathbf{v}_{i}\mathbf{v}_{i}^{H} \mathbf{h}_{\text{BS,DL}}^{(i)}}_{\widetilde{\mathbf{i}}} = \widetilde{\mathbf{I}} \cdot \mathbf{h}_{\text{BS,DL}}^{(i)}, \qquad (15)$$

where $\mathbf{v}_i, i=1,2,\ldots,N_b$ are right singular vectors of \mathbf{T} . Since $Trace(\widetilde{\mathbf{I}})=L$, $\mathbf{h}_{\mathrm{BS,DL}}^{(i)}$ cannot be fully recovered by only relying on the diagonal entries of $\widetilde{\mathbf{I}}$. If strong spatial correlation exists in the beam domain, we will need a recovery matrix $\widetilde{\mathbf{I}}$ with larger off-diagonal entries, representing the correlation between beams. Given the FDD UL/DL reciprocity in beam domain, by capturing the correlation between adjacent beam response magnitudes of UL CSI, it would be more reasonable to define a merging matrix \mathbf{T} which contains well-behaved right singular vectors such that $\sum_{i=0}^{N-1} ||\widetilde{\mathbf{Ih}}_{\mathrm{BS,DL}}^{(i)} - \mathbf{h}_{\mathrm{BS,DL}}^{(i)}||_{\mathrm{F}}^2$ can be minimized.

With the same design of the beam merging network in BSdualNet, the recovery network in BSdualNet-MN simply includes a series of matrix products. Thus, BSdualNet-MN is not only more interpretable, its computational complexity and required model memory are also lower.

V. UL CSI AIDED BEAM BASED PRECODING AND A RECONFIGURABLE CSI FEEDBACK FRAMEWORKS

Generally, the aforementioned methods perform better with high sparsity CSI in beam domain. Yet, such spatial sparsity may not hold for CSI of every propagation channels. For example, indoor propagation channels tend to exhibit rich multipaths with high angular spreads. This could lessen spatial sparsity and degrade recovery accuracy of DL CSI. Interestingly,

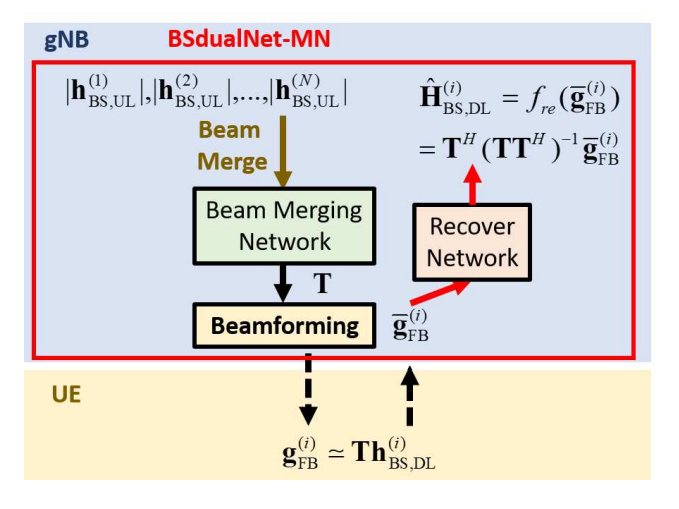


Fig. 8. Block Diagram of BSdualNet-MN.

however, such channels are alternatively characterized by large coherence bandwidth because of the dominance of low-delay paths dominate [28]. This means that for such channels, it is not necessary to have high CSI-RS density in frequency domain.

In this section, a reconfigurable CSI feedback framework will be described as a more flexible solution to reduce the number of pilots by selecting frequency reduction (FR) and beam reduction (BR) ratios. Instead of regarding feedback of each RB independently, as discussed in the signal model of Section II, we exploit the large coherence bandwidth and consider a joint UL feedback for a total of K RBs. By leveraging spectral coherence, we can further reduce the UL feedback overhead by applying an autoencoder network. In what follows, we elaborate on the reconfiguration of CSI-RS placement and the design of a learning-based CSI feedback framework, BSdualNet-FR.

A. Frequency Resource Reconfiguration

In modern wireless protocols, there are designated resource regions for CSI-RS placement [19]. Compatible with existing RS configurations, we can reduce the CSI-RS placement density along the frequency domain by a frequency reduction factor FR by placing pilots only at RB indices k=1,1+FR,1+2FR,...,1+(K-1)FR as shown in Fig. 9. We can also further reduce the required REs by a beam reduction factor of BR(= round(N_b/L)) by applying beam merging matrix T designed by using a three-dimensional (3-D) beam merging network with 3-D convolutional kernels as shown in Figs. 10 and 11. Jointly, the total REs for CSI-RS placement can be reduced by a factor of BR · FR. Thus, the total number of pilot REs becomes $N_b K/(BR \cdot FR)$.

The DL received signal vector $\mathbf{y}_{\mathrm{DL}}^{(i,k)} \in \mathbb{C}^{L \times 1}$ at the i-th UE in the k-th RB can be expressed as

$$\mathbf{y}_{\text{DL}}^{(i,k)} = \mathbf{S}_{\text{DL},L}^{(k)} \mathbf{T}^T \mathbf{h}_{\text{BS,DL}}^{(i,k)} + \mathbf{n}_{\text{DL}}^{(k)},$$
 (16)

where the superscript (i,k) denotes the UE and RB indexes, respectively. Following Section II, UE-i estimates beam re-

¹See Appendix

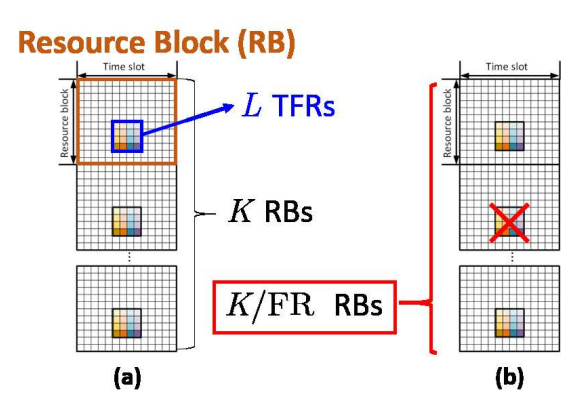


Fig. 9. Illustration of pilot number reduction. (Note that the color grids represent the designated TFRs in one of the pilot placement configurations defined in 5G specification [19].)

sponse vectors $\mathbf{g}_{\mathrm{FB}}^{(i,k)}, k=1,1+FR,...,1+(K-1)FR$ as a beam response matrix

$$\mathbf{G}_{\mathrm{FB}}^{(i)} = \left[\mathbf{g}_{\mathrm{FB}}^{(i,1)}, \mathbf{g}_{\mathrm{FB}}^{(i,1+FR)}, \ldots, \mathbf{g}_{\mathrm{FB}}^{(i,1+(K-1)FR)}\right] \in \mathbb{C}^{L \times K/FR}$$

where the estimates $\mathbf{g}_{\mathrm{FB}}^{(i,k)} = (\mathbf{S}_{\mathrm{DL},L}^{(k)})^{-1}\mathbf{y}_{\mathrm{DL}}^{(i,k)} \in \mathbb{C}^L$ are based on pilots reduced by FR.

B. BSdualNet-FR

For further reduction of UL feedback overhead, we compress the beam responses by implementing a frequency compression module (FCM) similar to an autoencoder. The FCM consists of an encoder at UE and decoder at gNB for CSI compression and recovery, respectively. The encoder consists of four 3×3 circular convolutional layers with 16,8,4 and 2 channels. Subsequently, an FC layer with $\left\lceil 2LK/(\text{CR}\cdot\text{FR})\right\rceil$ elements accounts for dimension reduction by a factor of $\text{CR}_{\text{eff}}=\text{BR}\cdot\text{FR}\cdot\text{CR}$ after reshaping. CR_{eff} and CR respectively denote the effective and feedback compression ratios. The FC layer output is sent to a quantization module which uses a trainable soft quantization function as proposed in [9] to generate feedback codewords.

At the gNB, the codewords from different UEs are forwarded into the decoder network of the FMC to recover their respective DL CSIs. The decoder first expands the dimension of the codewords to their original size of $2N_bK$. Reshaped into a size of $N_b \times K \times 2$, a codeword enters four 3×3 circular convolutional layers with with 16, 8, 4 and 2 channels to generate the FCM output. Note that the dimensions in both frequency and beam domains are already the same as our target output in this stage. The FCM output serves as an initial DL CSI estimate $\widehat{\mathbf{H}}_{\mathrm{BS,DL,ini}}^{(i)} \in \mathbb{C}^{N_b \times K}$ which is used to calculate the first loss

$$loss_1 = \sum_{i=0}^{N-1} ||\widehat{\mathbf{H}}_{BS,DL,ini}^{(i)} - \mathbf{H}_{BS,DL}^{(i)}||_2^2,$$
(17)

$$\widehat{\mathbf{H}}_{\mathrm{BS,DL,ini}}^{(i)} = f_{\mathrm{FMC,de}}(f_{\mathrm{FMC,en}}(\mathbf{G}_{\mathrm{FB}}^{(i)})). \tag{18}$$

Next, the combining network refines the initial estimate with the help of UL CSI magnitudes. The combining network

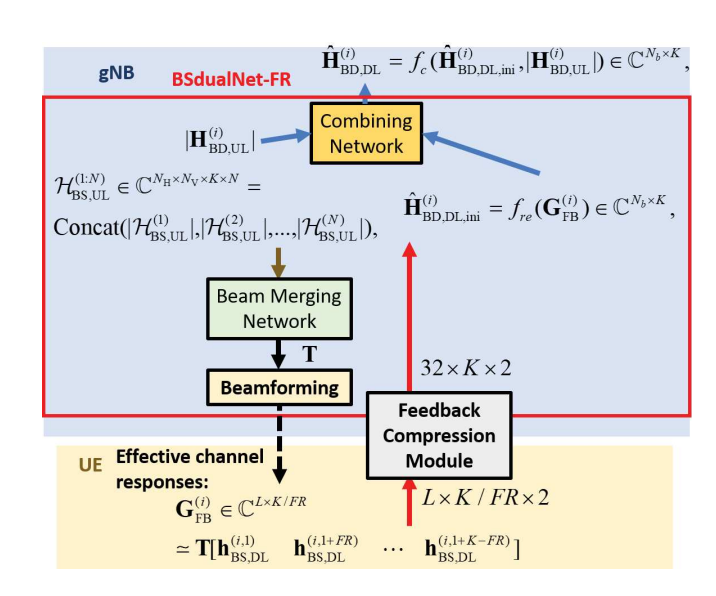


Fig. 10. Block Diagram of BSdualNet-FR.

first split the magnitude and the phase of the initial estimate before sending the initial estimate magnitudes and the UL CSI magnitudes into five residual blocks which are constructed by a shortcut and four circular convolutional layers with 16, 8, 4, 2 and 1 channels and activation functions for magnitude refinement. From there, the refined magnitudes of DL CSI and their corresponding phases form the final output $\widehat{\mathbf{H}}_{\mathrm{BS,DL}}^{(i)} \in \mathbb{C}^{N_b \times K}$ to determine the second loss function

$$loss_2 = \sum_{i=0}^{N-1} ||\widehat{\mathbf{H}}_{BS,DL}^{(i)} - \mathbf{H}_{BS,DL}^{(i)}||_2^2,$$
(19)

$$\mathbf{H}_{\mathrm{BS,UL}}^{(i)} = \left[\operatorname{vec}(\mathbf{H}_{\mathrm{BS,UL}}^{(i,1)}) \operatorname{vec}(\mathbf{H}_{\mathrm{BS,UL}}^{(i,2)}) \cdots \operatorname{vec}(\mathbf{H}_{\mathrm{BS,UL}}^{(i,K)}) \right]$$
(20)

$$\widehat{\mathbf{H}}_{\mathrm{BS,DL}}^{(i)} = f_c(\widehat{\mathbf{H}}_{\mathrm{BS,DL,ini}}^{(i)}, |\mathbf{H}_{\mathrm{BS,UL}}^{(i)}|), \tag{21}$$

The BSdualNet-FR is optimized by updating the network parameters Θ_{bm} , $\Theta_{FMC,en}$, $\Theta_{FMC,de}$ and Θ_c of the non-linear 3-D beam merging, FMC encoder/decoder, and combining networks f_{bm} , $f_{FMC,en}$, $f_{FMC,de}$ and f_c :

$$\mathop{\arg\min}_{\Theta_{\mathsf{bm}},\Theta_{\mathsf{FMC},\mathsf{en}},\Theta_{\mathsf{FMC},\mathsf{de}},\Theta_{\mathsf{c}}} \left\{\alpha \cdot \mathsf{loss}_1 + (1-\alpha) \cdot \mathsf{loss}_2\right\}$$

where hyperparameter α adjusts the weighting.

Note that the deep learning network contains many hyperbolic tangent activation functions and a soft quantization function which could lead to the gradient vanishing problem for parameters in those layers. To mitigate this problem, we suggest a two-stage training scheme for optimizing the proposed framework. In the first stage, we train the model by setting $\alpha=1$ for $N_{\rm first}$ epochs, freezing the combining network and focusing on finding the best beam merging matrix and encoding/decoding networks. In the second stage, we change $\alpha=0.1$ and focus on refining the final estimates with the aid of UL CSI magnitudes. Using the elbow method [29], we

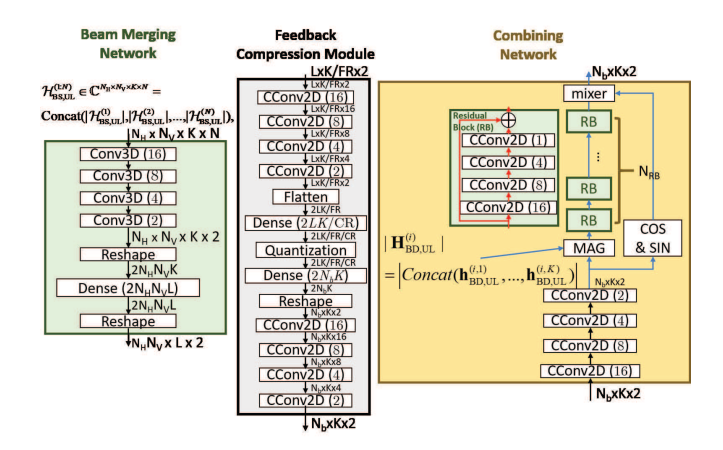


Fig. 11. Network design of BSdualNet-FR.

found that $N_{\rm first}=30$ is usually sufficient to obtain a good tradeoff.

VI. EXPERIMENTAL EVALUATIONS

A. Experiment Setup

In our numerical test, we consider both indoor and outdoor cases. Using channel model software, we position a gNB of height equal to 20 m at the center of a circular cell with a radius of 30 m for indoor and 200 m for outdoor environment. We equip the gNB with a $8\times 4(N_H\times N_V)$ UPA for communication with single antenna UEs. UPA elements have half-wavelength uniform spacing. The number of residual blocks in the combining network is set to $N_B=5$ throughout.

For our proposed model and other competing models, we set the number of epochs to 300 and 1500, respectively. We use batch size of 200. For our model, we start with learning rate of 0.001 before switching to 10^{-4} after the 100-th epoch. Using the channel simulator, We generate several indoor and outdoor datasets, each containing 100,000 random channels. 57,143 and 28,571 random channels are for training and validation. The remaining 14,286 channels are test data for performance evaluation. For both indoor and outdoor, we use the QuaDRiGa simulator [27] using the scenario features given in 3GPP TR 38.901 Indoor and 3GPP TR 38.901 UMa at 5.1-GHz and 5.3-GHz, and 300 and 330 MHz of UL and DL with LOS paths, respectively. For both scenarios, 1024 subcarriers with a 15K-Hz spacing are considered for each subband. Here, we assume UEs are capable of perfect channel estimation. We set antenna type to omni. We use normalized MSE as the performance metric

$$\frac{1}{ND} \sum_{d=1}^{D} \sum_{n=1}^{N} \left\| \widehat{\mathbf{H}}_{\text{BS,DL},d}^{(i)} - \mathbf{H}_{\text{BS,DL},d}^{(i)} \right\|_{\text{F}}^{2} / \left\| \mathbf{H}_{\text{BS,DL},d}^{(i)} \right\|_{\text{F}}^{2}, \quad (22)$$

where the number D and subscript d denote the total number and index of channel realizations, respectively.

B. Testing Different Numbers of Available REs

We evaluate the performance of CSI recovery by adopting the proposed encoder-free CSI feedback frameworks,

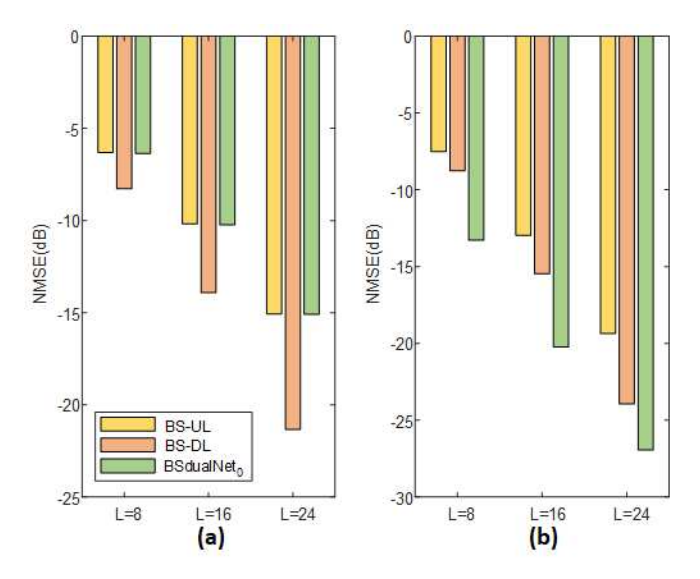


Fig. 12. NMSE performance of BS-UL, BS-DL, and BSdualNet $_0$ for different TFRs L in (a) indoor, (b) outdoor scenarios.

BSdualNet₀, BSdualNet and BSdualNet-MN. To test the efficacy without considering quantization, we first compare BSdualNet₀ with two heuristic approaches (denoted as BS-UL and BS-DL) that recover DL CSIs according to *L* beam responses where the beams are selected according to the UL and DL CSI magnitudes, respectively. Note that BS-UL should serve as the lower bound of BSdualNet₀ since BSdualNet₀ is equivalent to refine the result of BS-UL with an additional combining network.

Figs. 12 (a) and (b) provide the NMSE performance for different number of available REs L in an RB for BSdualNet₀, BS-UL and BS-DL in both indoor and outdoor scenarios, respectively. The results show that BSdualNet₀ delivers better performance than BS-UL and also BS-DL in outdoor scenario owing to the high spatial correlation in beam domain. Because of the high angle spread induced by the more complex multi-path environment in indoor scenarios, the combining network in BSdualNet₀ only marginally improve the recovery performance.

Figs. 13 (a) and (b) illustrate the NMSE performance for different number L of REs within a RB for BSdualNet₀, BSdualNet and BSdualNet-MN for both indoor and outdoor channels, respectively. We can observe the benefits of the beam merging matrix \mathbf{T} especially in outdoor cases. Furthermore, instead of using a convolution-layer based combining network, changing the combining function as a minimum-norm solution yields a significant performance improvement in both indoor and outdoor scenarios. Since minimum-norm solution directly uses the beam merging matrix \mathbf{T} , it becomes more efficient to decouple the superposition of weighted beam responses by minimizing the MSE of DL CSIs.

C. Performance for Different Numbers of UEs

Similar to our beam merging matrix **T**, measurement matrix in compressive sensing based frameworks [30], [31] also

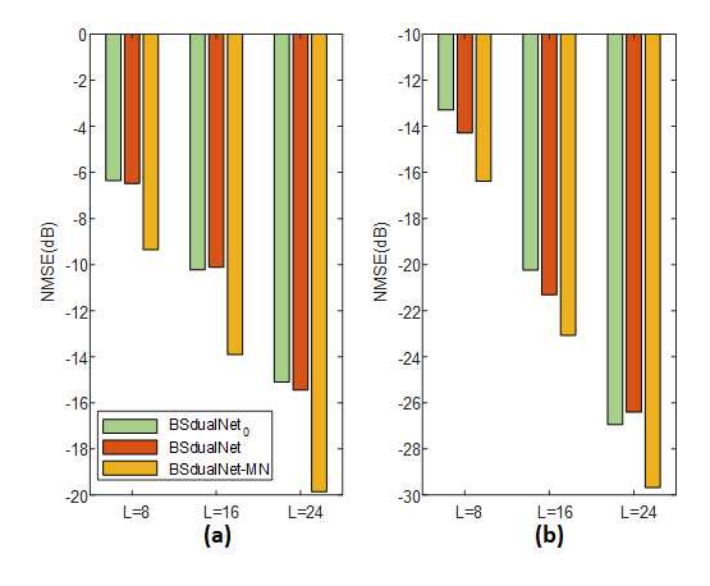


Fig. 13. NMSE performance of BSdualNet $_0$, BSdualNet, and BSdualNet-MN for different TFRs L in (a) indoor, (b) outdoor scenarios.

functions to shrink the dimension of original data and derive a better representation for their sparsity that can be easier to recover. To demonstrate the relative performance of the proposed frameworks, we also compare with two successful compressive approaches ISTA [30] and ISTA-Net [31]:

- Iterative Shrinkage-Thresholding Algorithm (ISTA): Its regularization parameter and maximum iteration number are set to 0.5 and 3000, respectively.
- **ISTA-Net**: The phase and epoch numbers are set to 5 and 1000, respectively.

Figs. 14 (a) and (b) provide the NMSE performance comparison for different numbers of UEs N for L=8 REs in a RB for BSdualNet, BSdualNet-MN, ISTA and ISTA-Net and under indoor and outdoor scenarios, respectively. From the results, we observe the clear performance degradation for BSdualNet and BSdualNet-MN as UE number grows. This is intuitive since it is difficult to find an optimum beam merging matrix for all active UEs. Fortunately, for most cases, the performance degradation tends to saturate after the UE number exceeds a certain number typically less than 10 for BSdualNet-MN.

Our tests show that both BSdualNet and BSdualNet-MN deliver better performance over ISTA and ISTA-Net under different UE numbers. Our heuristic insight is that measurement matrix in ISTA and ISTA-Net is unknown at recovery whereas the beam merging matrix is designed by the gNB and can be explicitly utilized by the recovery decoders of BSdualNet and BSdualNet-MN.

D. CSI-RS Configurations and Compression Ratios

We consider a 5.76 MHz subband (i.e., 32 RBs each of bandwidth 180K-Hz). Each codeword element uses 8 quantization bits. To comprehensively evaluate BSdualNet-FR, The two tables in Fig. 15 and Fig. 16 provide the NMSE performance of BSdualNet-FR against different CSI-RS configurations and compression ratios in outdoor and

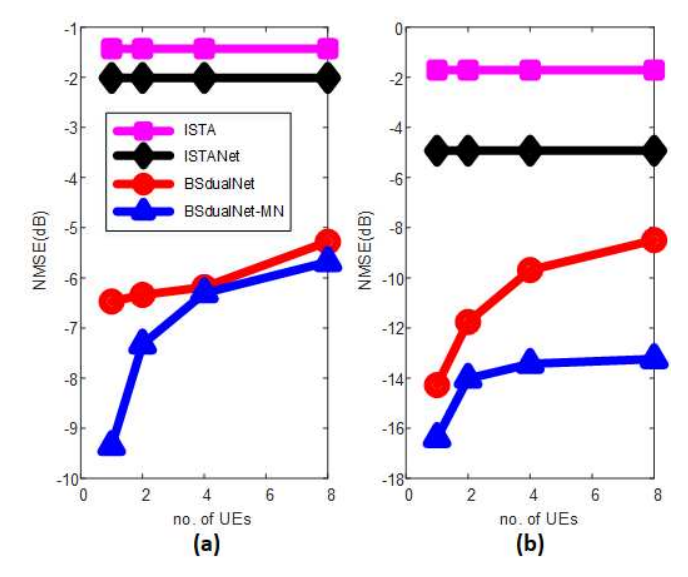


Fig. 14. NMSE performance for different number of UEs N in (a) indoor, (b) outdoor scenarios.

indoor scenarios, respectively. We apply the same background color on results with the same pilot and feedback overhead reduction ratios.

Since outdoor channels generally exhibit stronger sparsity and larger delay spread respectively in beam and delay domains, we observe a slight performance degradation with BR increase as opposed to FR increase. Importantly, for BR=4, there is a clear performance loss even when using the same pilot and feedback overhead reduction ratio. Despite the channel sparsity, with the use of half-wavelength antenna spacing (i.e., Nyquist sampling in spatial domain), the overly aggressive compression in beam domain cause too much information loss to recovery at the gNB. For indoor channels, we observe a slight performance degradation when increasing FR instead of BR because of larger angular and shorter delay spread of indoor CSI.

E. Effective Compression Ratio CR_{eff}

As benchmarks, we also compare BSdualNet-FR with CsiNet-Pro [7] and another successful method DualNet-MP [11]. The newly proposed DualNet-MP also exploits FDD reciprocity by incorporating UL CSI magnitude as side information at CSI decoder of gNB. Table I presents the three way comparison of NMSE for CsiNet-Pro, DualNet-MP, and BSdualNet-FR under different values of effective compression ratio CReff in indoor and outdoor cases. Benefiting from the UL CSI magnitudes, both BSdualNet-FR and DualNet-MP can outperform CsiNet-Pro in most cases. Interesting, better utilization of UL CSI by BSdualNet-FR provides better performance than DualNet-MP. Although the performance gain becomes less impressive for higher CR_{eff}, the additional benefit of the BSdualNet-FR framework is the reduction of REs for DL CSI-RS by a factor of BR · FR that allows gNB to reconfigure the CSI-RS placement to enhance the DL spectrum efficiency.

 $TABLE\ I$ NMSE performance of different CSI feedback frameworks at different CR_{EFF}

	CsiNet-Pro		DualNet-MP		BSdualNet-FR					
CR _{eff}	Indoor	Outdoor	Indoor	Outdoor	Indoor	Outdoor				
4	-24.2	-13	-27.3 -19.1	10.1	-34.6	-19.8				
4	-24.2	-13		-19.1	(FR = 1, BR = 1)	(FR = 1, BR = 1)				
8	-20.8	-12.5	-20.9	-16.4	-34.5	-16.5				
0	-20.6	-12.3	-20.9	-10.4	(FR = 4, BR = 1)	(FR = 1, BR = 1)				
16	14.4	-14.4	-11.8	14.4 11.9	20.2	-20.2 -1	12.2	-13.3	-27.2	-13.3
10	-14.4	-11.0	-20.2	-13.3	(FR = 8, BR = 1)	(FR = 1, BR = 2)				
32	-13.2	-8.6	-16.8	-11	-17.4	-11				
					(FR = 8, BR = 1)	(FR = 2, BR = 2)				

CR = 2	BR=1 (L=32)	BR=2 (L=16)	BR=4 (L=16)		
FR=2	-34.45	-10.16	-6.66		
FR=4	<u>-34.5</u>	-10.2			
FR=8	<u>-27.2</u>				
CR = 4	BR = 1 (L=32)	BR = 2 (L=16)	BR = 4 (L=8)		
FR = 1	-34.63	-10	-6.66		
FR = 2	-34.06	-10.12	-6.85		
FR = 4	-27.03	-10.25			
FR = 8	<u>-17.41</u>				
0 0					
CR = 8	BR=1 (L=32)	BR=2 (L=16)	BR=4 (L=8)		
FR=1	-33.46	-10.14	-6.75		
FR=2	-26	-10.15			
FR=4	-17.31				
	-				
	$CR_{eff} = 4$ $CR_{eff} = 16$				

Fig. 15. NMSE performance of BSdualNet-FR for different CSI-RS placement configurations in indoor scenarios. (The results with the same effective compression ratio are denoted as the same color. The best performance at the same effective compression ratio is denoted by bold fonts with underline.)

CR = 2	BR=1 (L=32)	BR=2 (L=16)	BR=4 (L=16)		
FR=2	-18.41	-15.21	-12.28		
FR=4	-15.73	-12.94			
FR=8	-10.78				
			×		
CR = 4	BR = 1 (L=32)	BR = 2 (L=16)	BR = 4 (L=8)		
FR = 1	<u>-19.78</u>	-15.43	-10.89		
FR = 2	-16.08	-13.19	-9.98		
FR = 4	-13.18	-10.79			
FR = 8	-9.642				
CR = 8	BR=1 (L=32)	BR=2 (L=16)	BR=4 (L=8)		
FR=1	<u>-16.54</u>	<u>-13.3</u>	-10.07		
FR=2	-13.28	<u>-10.95</u>			
FR=4	-9.30				
	$CR_{eff} = 4$ $CR_{eff} = 16$				
	$CR_{eff} = 8$ $CR_{eff} = 32$				

Fig. 16. NMSE performance of BSdualNet-FR for different CSI-RS placement configurations in outdoor scenarios. (The results with the same effective compression ratio are denoted as the same color. The best performance at the same effective compression ratio is denoted by bold fonts with underline.)

F. Complexity: FLOPs and Parameters

Most UEs have stronger memory, computation, and power constraints. The system design favors light-weight and simpler encoders for deployment at UEs. In comparison with the baseline CsiNet Pro, Table II shows dimension reduction in frequency and beam domains and smaller input size of our encoder/decoder architecture. BSdualNet-FR provides significant reduction in terms of FLOPs and the number of model parameters. Similarly, if the total reduction factor $FR \cdot BR \geq 2$, BSdualNet-FR shows lower complexity than DualNet-MP.

VII. CONCLUSIONS

This work presents a new deep learning framework for CSI estimation in massive MIMO downlink. Leveraging UL CSI estimate to reduce its CSI-RS resources, the gNB designs a beam merging matrix based on UL channel magnitude information to transform DL CSI observation at UEs into a lower dimensional representation that is easier for feedback

and recovery. We further develop an efficient minimum-norm CSI recovery network to improve recovery accuracy. Our new framework does not deploy training deep learning models at UEs, thereby lowering UE complexity and power consumption. We achieve further reduction of DL CSI training and feedback overhead, by introducing a reconfigurable CSI-RS placement. Test results demonstrate significant improvement of CSI recovery accuracy and reduction of both DL CSI training and UL feedback overheads.

APPENDIX

Proof of Eq. (15):

For an $L \times N_b$ merging matrix \mathbf{T} with $L < N_b$, we have an underdetermined linear problem $\mathbf{y} = \mathbf{T}\mathbf{x}$. The minimum norm solution is simply

$$\mathbf{x}_{mn} = \mathbf{T}^H (\mathbf{T}\mathbf{T}^H)^{-1} \mathbf{T} \mathbf{x}, \tag{A.1}$$

TABLE II
COMPARISON OF PARAMETERS AND FLOPS AT ENCODER.

	CsiNet-Pro		DualNet-MP		BSdualNet-FR	
CR_{eff}	Parameters	FLOPs	Parameters	FLOPs	Parameters	FLOPs
4	1M	4.23M	0.54M	4.2M	1M/(FR*BR)	(2.1 + 2.1/(FR*BR))M
8	534K	2.12M	280K	2.2M	534K/(FR*BR)	(1.1 + 1/(FR*BR))M
16	272K	1.08M	140K	1.1M	272K/(FR*BR)	(0.55 + 0.5/(FR*BR))M
32	140K	0.56M	82K	0.6M	140K/(FR*BR)	(0.27 + 0.26/(FR*BR))M

Based on singular value decomposition of T by

$$\mathbf{T} = \mathbf{U} \begin{bmatrix} \mathbf{\Sigma} & \mathbf{0} \end{bmatrix} \mathbf{V}^H, \tag{A.2}$$

where \mathbf{U} and \mathbf{V} respectively are left and right singular matrices corresponding to the $L \times L$ diagonal Σ of nonzero singular values. Let $\mathbf{V} = [\mathbf{v}_1 \ \mathbf{v}_2 \ \cdots \mathbf{v}_{N_b}]$ denote the corresponding right singular vectors. It is clear that

$$\mathbf{T}^{H}(\mathbf{T}\mathbf{T}^{H})^{-1}\mathbf{T} = \mathbf{V} \begin{bmatrix} \mathbf{I}_{L \times L} & \mathbf{0} \\ \mathbf{0} & \mathbf{0} \end{bmatrix} \mathbf{V}^{H} = \sum_{i=1}^{L} \mathbf{v}_{i} \mathbf{v}_{i}^{H} \quad (A.3)$$

Define a matrix $\widetilde{\mathbf{I}} = \sum_{i=1}^{L} \mathbf{v}_i \mathbf{v}_i^H$. The minimum-norm solution is simply

$$\mathbf{x}_{mn} = \sum_{i=1}^{L} \mathbf{v}_i \mathbf{v}_i^H \mathbf{x} = \widetilde{\mathbf{I}} \cdot \mathbf{x}. \tag{A.4}$$

Since the singular vectors $\{\mathbf{v}_i\}$ are orthonormal, i.e., $\mathbf{v}_i^H \mathbf{v}_i = 1$, it is clear that

$$\begin{aligned} \operatorname{Trace}\{\widetilde{\mathbf{I}}\} &= \sum_{i=1}^{L} \operatorname{Trace}\{\mathbf{v}_{i} \mathbf{v}_{i}^{H}\} \\ &= \sum_{i=1}^{L} \operatorname{Trace}\{\mathbf{v}_{i}^{H} \mathbf{v}_{i}\} \\ &= \sum_{i=1}^{L} 1 = L \end{aligned} \tag{A.5}$$

in which the equality of Eq. (A.5) holds because $Trace\{AB\} = Trace\{BA\}$.

VIII. ACKNOWLEDGEMENT

The authors would like to acknowledge Mason del Rosario for his useful discussions which helped the authors better understand of pilot placement and channel truncation.

REFERENCES

- C.-H. Lin, S.-C. Lin, and E. Blasch, "TULVCAN: Terahertz Ultrabroadband Learning Vehicular Channel-aware Networking," in *IEEE INFOCOM workshop*, May 2021, pp. 1–6.
- [2] C. Wen, W. Shih, and S. Jin, "Deep Learning for Massive MIMO CSI Feedback," *IEEE Wirel. Commun. Lett.*, vol. 7, no. 5, pp. 748–751, 2018.
- [3] Y. Sun, W. Xu, L. Liang, N. Wang, G. Y. Li, and X. You, "A Lightweight Deep Network for Efficient CSI Feedback in Massive MIMO Systems," *IEEE Wirel. Commun. Lett.*, vol. 10, no. 8, pp. 1840–1844, 2021.
- [4] S. Ji and M. Li, "CLNet: Complex Input Lightweight Neural Network Designed for Massive MIMO CSI Feedback," *IEEE Wirel. Commun. Lett.*, vol. 10, no. 10, pp. 2318–2322, 2021.
- [5] Z. Lu, J. Wang, and J. Song, "Multi-resolution CSI Feedback with Deep Learning in Massive MIMO System," in *IEEE Intern. Conf. Communications (ICC)*, 2020, pp. 1–6.

- [6] J. Guo et al., "Convolutional Neural Network-Based Multiple-Rate Compressive Sensing for Massive MIMO CSI Feedback: Design, Simulation, and Analysis," *IEEE Trans. Wirel. Commun.*, vol. 19, no. 4, pp. 2827–2840, 2020.
- [7] Z. Liu, M. Rosario, and Z. Ding, "A Markovian Model-Driven Deep Learning Framework for Massive MIMO CSI Feedback," *IEEE Trans. Wirel. Commun.*, 2021, early access.
- [8] J. Guo et al., "DL-based CSI Feedback and Cooperative Recovery in Massive MIMO," arXiv preprint arXiv:2003.03303, 2020.
- [9] Z. Liu, L. Zhang, and Z. Ding, "An Efficient Deep Learning Framework for Low Rate Massive MIMO CSI Reporting," *IEEE Trans. Commun.*, vol. 68, no. 8, pp. 4761–4772, 2020.
- [10] —, "Exploiting Bi-Directional Channel Reciprocity in Deep Learning for Low Rate Massive MIMO CSI Feedback," *IEEE Wirel. Commun. Lett.*, vol. 8, no. 3, pp. 889–892, 2019.
- [11] Y.-C. Lin, Z. Liu, T.-S. Lee, and Z. Ding, "Deep Learning Phase Compression for MIMO CSI Feedback by Exploiting FDD Channel Reciprocity," *IEEE Wireless Commun. Lett.*, vol. 10, no. 10, pp. 2200– 2204, 2021.
- [12] Z. Zhong, L. Fan, and S. Ge, "FDD Massive MIMO Uplink and Downlink Channel Reciprocity Properties: Full or Partial Reciprocity?" in *IEEE GLOBECOM*, Dec. 2020, pp. 1–5.
- [13] Y. Ding and B. D. Rao, "Dictionary Learning-based Sparse Channel Representation and Estimation for FDD Massive MIMO Systems," *IEEE Trans. Wirel. Commun.*, vol. 17, no. 8, pp. 5437–5451, 2018.
- [14] X. Zhang, L. Zhong, and A. Sabharwal, "Directional Training for FDD Massive MIMO," *IEEE Trans. Wirel. Commun.*, vol. 17, no. 8, pp. 5183– 5197, 2018.
- [15] W. Shen et al., "Channel Feedback Based on AoD-adaptive Subspace Codebook in FDD Massive MIMO Systems," IEEE Trans. Commun., vol. 66, no. 11, pp. 5235–5248, 2018.
- [16] Intel, "On NR Type I Codebook," TSG RAN WG1 No. 88 R1-1702205, 2021.
- [17] Samsung, "Type II CSI Reporting," TSG RAN WG1 No. 89 R1-1707962, 2021.
- [18] M. Chen et al., "Deep Learning-based Implicit CSI Feedback in Massive MIMO," arXiv preprint arXiv:2105.10100, 2021.
- [19] 3GPP, "NR; Physical Channels and Modulation," 3rd Generation Partnership Project (3GPP), Technical Specification (TS) 38.211, June 2020, version 16.6.0.
- [20] Y.-C. Lin, T.-S. Lee, and Z. Ding, "Deep Learning for Partial MIMO CSI Feedback by Exploiting Channel Temporal Correlation," in *Asilomar Conf. Signals, Syst., Comput.*, 2021, pp. 345–350.
- [21] J. Guo, C.-K. Wen, and S. Jin, "CAnet: Uplink-aided Downlink Channel Acquisition in FDD Massive MIMO using Deep Learning," *IEEE Trans. Commun.*, 2021, early access.
- [22] G. Morozov, A. Davydov, and V. Sergeev, "Enhanced CSI Feedback for FD-MIMO with Beamformed CSI-RS in LTE-A Pro Systems," in VTC-Fall, 2016, pp. 1–5.
- [23] R. L. Haupt, "Array Beamforming," Timed Arrays: Wideband and Time Varying Antenna Arrays, pp. 78–94, 2015.
- [24] 3GPP, "Beam management," 3GPP, Technical Report (TR) 38.802, Sep. 2017, version 16.6.0.
- [25] C.-H. Lin, W.-C. Kao, S.-Q. Zhan, and T.-S. Lee, "BsNet: A Deep Learning-Based Beam Selection Method for mmWave Communications," in VTC-Fall, 2019, pp. 1–6.
- [26] Y.-C. Lin, T.-S. Lee, Y.-H. Pan, and K.-H. Lin, "Low-Complexity High-Resolution Parameter Estimation for Automotive MIMO Radars," *IEEE Access*, vol. 8, pp. 16127–16138, 2020.
- [27] S. Jaeckel et al., "QuaDRiGa: A 3-D Multi-Cell Channel Model with Time Evolution for Enabling Virtual Field Trials," *IEEE Trans. Antennas and Propag.*, vol. 62, no. 6, pp. 3242–3256, 2014.

- [28] W. Debaenst, A. Feys, I. Cuiñas, M. G. Sánchez, and J. Verhaevert, "RMS Delay Spread vs. Coherence Bandwidth from 5G Indoor Radio Channel Measurements at 3.5 GHz Band." Sensors, vol. 20, no. 3, 2020.
- Channel Measurements at 3.5 GHz Band," *Sensors*, vol. 20, no. 3, 2020.

 [29] D. J. Ketchen and C. L. Shook, "The Application of Cluster Analysis in Strategic Management Research: An Analysis and Critique," *Strategic Management Journal*, vol. 17, no. 6, pp. 441–458, 1996.

 [30] A. Beck and N. Teboulle, "A Fast Iterative Shrinkage-Thresholding
- [30] A. Beck and N. Teboulle, "A Fast Iterative Shrinkage-Thresholding Algorithm for Linear Inverse Problems," *Society for Industrial and Applied Mathematics*, vol. 2, no. 1, p. 183–202, Mar. 2009.
- [31] J. Zhang and B. Ghanem, "ISTA-Net: Interpretable Optimization-Inspired Deep Network for Image Compressive Sensing," in *IEEE CVPR*, 06 2018, pp. 1828–1837.